Ferroelectric Control of the Conduction at the $LaAlO_3$/$SrTiO_3$ Heterointerface

Vu Thanh Tra, Jhih-Wei Chen, Po-Cheng Huang, Bo-Chao Huang, Ye Cao, Chao-Hui Yeh, Heng-Jui Liu, Eugene A. Eliseev, Anna N. Morozovska, Jiunn-Yuan Lin, Yi-Chun Chen, Ming-Wen Chu, Po-Wen Chiu, Ya-Ping Chiu, Long-Qing Chen, Chung-Lin Wu,* and Ying-Hao Chu*

Complex oxide heterointerfaces have emerged as one of the most exciting subjects in condensed matter, owing to their unique physical properties and new possibilities for next-generation electronic devices.[1,2] In the push for practical applications, it is desirable to have the ability to modulate the interface functionalities by an external stimulus. In this Communication, we propose a generic approach in which a functional layer is inserted into the heterostructure to acquire non-volatile control of the intriguing properties at oxide interfaces. The $LaAlO_3$/$SrTiO_3$ (LAO/STO) interface serves as a model system in which a highly mobile quasi-two-dimensional electron gas (2DEG) forms between two band insulators,[3,4] exhibiting 2D superconductivity[5] and unusual magnetotransport properties.[6] Although a modulation of the carrier density and mobility of the LAO/STO interface has been achieved using the electric field effect,[7–9] it is essential to extend the control concepts to gain non-volatile and reversible capabilities for practical applications. Recently, non-volatile modification of the local conduction at the LAO/STO interface has been demonstrated by scanning probe techniques.[10–12] Several possible mechanisms have been proposed to explain this interesting behavior based on the electrostatic effects attributed to either induced ferroelectricity or surface charge.[13,14] In the study reported here, we added a ferroelectric $Pb(Zr_{0.2}Ti_{0.8})O_3$ (PZT) layer near the LAO/STO interface. The ferroelectric polarization of the PZT layer serves as a control parameter to modulate the 2DEG conducting behavior. The as-grown polarization (P_{up} state) leads to charge depletion and consequently low conduction. Switching the polarization direction (P_{down} state) results in charge accumulation and enhances the conduction at the LAO/STO interface. The origin of this modulation is attributed to a change in the electronic structure due to the ferroelectric polarization states, evidenced by X-ray photoelectron spectroscopy (XPS) and cross-sectional scanning tunneling microscopy/spectroscopy (XSTM/S). Control of the conduction at this oxide interface suggests that the concept can be generalized for other oxide systems to design functional interfaces.

In order to understand the influence of ferroelectricity on the LAO/STO interface experimentally, we first carried out electrical transport measurements on the heterostructure (**Figure 1**a), in which the PZT layer with the spontaneous polarization P_{PZT} functions as a polarized dielectric slab to modulate the conduction of the LAO/STO heterointerface. Figure 1b shows the sheet resistance versus temperature (*R*–*T* curves) of the PZT/LAO/STO samples with various PZT layer thicknesses (0–40 nm), while the LAO thickness was fixed (6 u.c., where u.c. stands for unit cell). The *R*–*T* curves for these samples show that the sheet resistance at room temperature is low (ca. 23 kΩ/sq) and decreases with temperature, showing metallic behavior. For the samples with PZT on top, the ferroelectric effect sets in and the sheet resistance starts increasing with PZT thickness, showing the strong impact of the intrinsic

V. T. Tra, Prof. J.-Y. Lin
Institute of Physics
National Chiao Tung University
Hsinchu, 30010, Taiwan, ROC
E-mail: ago@nctu.edu.tw
J.-W. Chen, Prof. Y.-C. Chen, Prof. C.-L. Wu
Department of Physics
National Cheng Kung University
Tainan, 70101, Taiwan, ROC
E-mail: clwuphys@mail.ncku.edu.tw
P.-C. Huang, B.-C. Huang, Prof. Y.-P. Chiu
Department of Physics
National Sun Yat-Sen University
Kaohsiung, 80424, Taiwan, ROC
Y. Cao, Prof. L. Q. Chen
Department of Materials Science and Engineering
Pennsylvania State University
University Park, PA 16802, USA
C.-H. Yeh, Prof. P.-W. Chiu
Department of Electrical Engineering
National Tsing Hua University
Hsinchu, 30013,Taiwan, ROC
E. A. Eliseev, Prof. A. N. Morozovska
Institute of Problems of Material Sciences
and Institute of Physics
National Academy of Science of Ukraine
Kiev, Ukraine
Prof. M.-W. Chu
Center for Condensed Matter Sciences
National Taiwan University
Taipei, 10617, Taiwan, ROC
Dr. H.-J. Liu, Prof. Y. H. Chu
Department of Materials Science and Engineering
National Chiao Tung University
Hsinchu, 30010, Taiwan, ROC

DOI: 10.1002/adma.201300757

© 2013 WILEY-VCH Verlag GmbH & Co. KGaA, Weinheim

COMMUNICATION

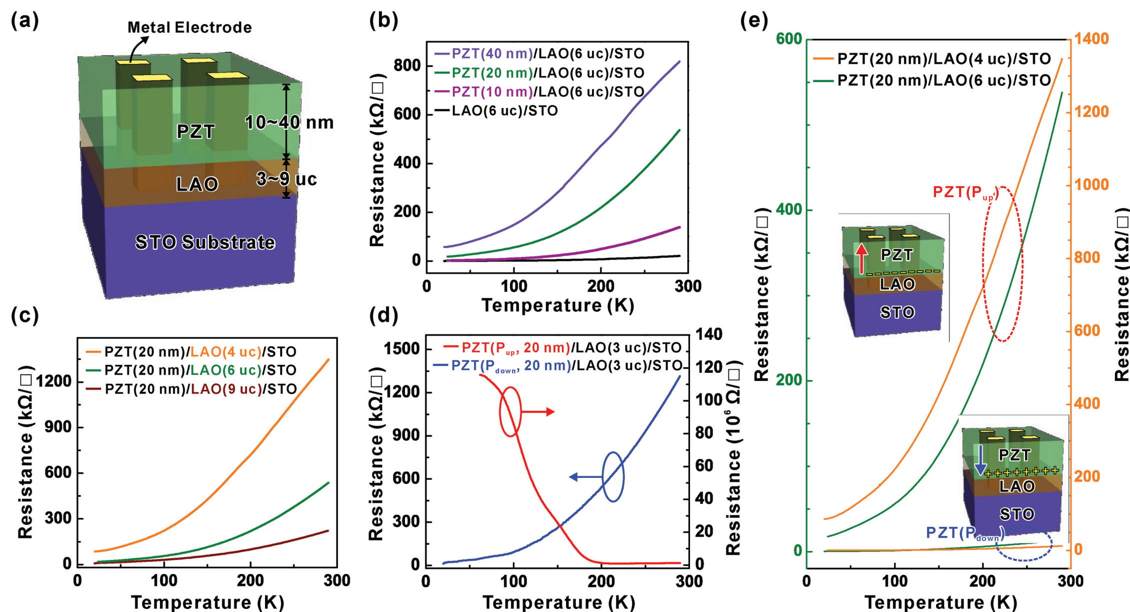

Figure 1. Transport measurement of PZT/LAO/STO devices: a) Sketch of the samples and the contact configurations down to the LAO/STO interface formed by the e-beam lithography method. b) Temperature dependence of the sheet resistance, R_s, for different values of PZT thickness on an n-type LAO/STO conducting interface. c) Influence of LAO thickness on the electronic properties of the PZT/LAO/STO devices while keeping PZT thickness constant at 20 nm on top of the LAO/STO heterointerface. d) Sheet resistance measured as a function of temperature for PZT (20 nm)/LAO (3 u.c.)/STO as grown with natural polarization (P_{up}) and after switching the polarization to the down state (P_{down}). e) Modulation of sheet resistance from high to low resistance states of two samples, PZT (20 nm)/LAO (6 u.c.)/STO and PZT (20 nm)/LAO (4 u.c.)/STO, corresponding to natural polarization (P_{up}) and after switching (P_{down}), respectively.

polarization (P_{up}) of PZT on electron conduction at the interface. This is anticipated since the ferroelectric field effect provides one more degree of freedom to compensate the charge imbalance at the interface.[15] We also conducted transport measurements on the samples with different LAO thickness, while PZT thickness was kept constant (20 nm) (Figure 1c). Several studies suggested a critical LAO thickness (4 u.c.) for the formation of the 2DEG at this interface.[7] Under such circumstances, all the samples with LAO above a critical thickness behave like a metal. The sheet resistance decreases when the temperature is lowered and increases when the thickness of LAO is reduced. These resistance changes can be rationalized in the framework of polarity discontinuity, which leads to an abated built-in electric field when the LAO thickness is reduced. Based on the experimental results, we are able to estimate that the sheet resistance increases by an order of magnitude when the LAO is decreased by 1 u.c. Moreover, the increase of sheet resistance with decreasing gap thickness (h) is in qualitative agreement with our simulation result (shown in the Supporting Information, Figure B2c).

The transport measurements provided clear insight into the influence of the ferroelectric effect on the LAO/STO interface, and now the question is raised: Can one modulate the interface conduction by ferroelectricity? We employed the scanning probe technique to switch the ferroelectric polarization of the samples. After the ferroelectric polarization had been switched, bipolar-resistance behavior was observed in the PZT/LAO/STO devices. Figure 1e shows the R–T curves of LAO (4 u.c.) and LAO (6 u.c.) after PZT (20 nm) with two different ferroelectric polarization directions had been deposited on top of the 2DEG. The sheet resistance in the initial polarization state (P_{up}) is rather high. After the polarization was flipped to the opposite direction (P_{down}), the sheet resistance became much lower. The sheet resistance modulating the conductivity at the LAO/STO interface with different polarization states of PZT can reach more than two orders of magnitude difference for the PZT (20 nm)/LAO (4 u.c.)/STO sample at room temperature. Another intriguing feature here is the switching of an insulating state to a conducting state. The PZT/LAO (3 u.c.)/STO typically shows insulating behavior. Switching the polarization can change the transport behavior from insulating to metallic, suggesting non-volatile control of the metal–insulator transition with ferroelectricity (Figure 1d). The transport measurements indicate that the ferroelectric field effects can not only modulate the conduction but also switch the conducting state.

In order to understand the fundamental mechanism behind this intriguing behavior, it is crucial to investigate the ferroelectric manipulation of electronic structure at the LAO/STO heterointerface. Here, ferroelectric-pattern-assisted XPS was used to probe the reversible interfacial electrostatics and its affected electronic structures. In the ferroelectric PZT/LAO/STO heterointerface with a naturally upward-polarized PZT layer, the polarization was reversed by the scanning probe technique (probe voltage set to 8 V) to obtain a downward polarization area of about 1 mm^2, which is larger than the X-ray beam size of about 400 μm^2. This ferroelectric-pattern-assisted spectral technique allows us to study the polarization reversal using the same sample. Consequently, we do not have to compare the polarization states in two different samples and we can avoid all discussion about sample quality and other differences. As

© 2013 WILEY-VCH Verlag GmbH & Co. KGaA, Weinheim

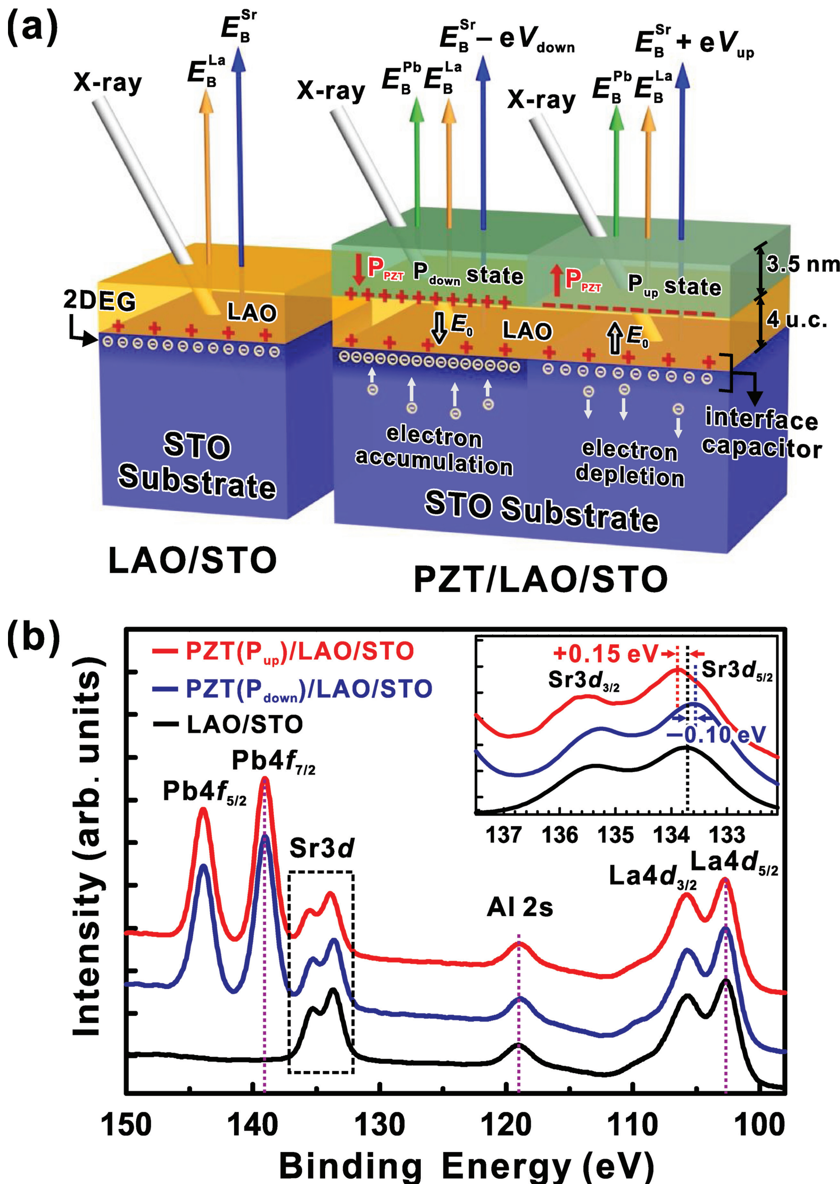

Figure 2. XPS study of the upward/downward ferroelectric polarization PZT/LAO/STO and LAO/STO heterostructures. a) Schematic illustration of the photoemission spectroscopy measurement on the upward (P_{up})/downward (P_{down}) polarized PZT/LAO/STO heterostructure and the bare LAO/STO sample. The Pb 4f, La 4d, and Sr 3d emission (indicated by green, yellow, and blue arrows, respectively) are captured from the PZT, LAO, and STO layers separately (indicated by green, yellow, and blue blocks, respectively). b) The XPS spectra taken from the PZT/LAO/STO and bare LAO/STO samples. The photoelectron peaks are aligned at the same energy for Pb 4f and La 4d (indicated by purple vertical dashed lines), but the Sr 3d core level has a significant binding energy downshift from 0.15 to –0.1 eV when the P_{up} ferroelectric PZT is switched to P_{down} (see inset).

depicted in **Figure 2**a, positive (P_{down} state) and negative (P_{up} state) bound charge sheets at the bottom of the PZT layer affect the conducting LAO/STO heterointerface, leading to an accumulation or depletion of free electrons in the STO layer. Consequently, in distinct ferroelectric patterns with reversed electric configuration, two interfacial capacitors having different electric fields inside were constructed separately with a top sheet of positive bound charges and a bottom sheet of negative mobile electrons. In previous studies, the binding energies of core-level photoelectrons emitted from the epitaxial thin films and substrate were found to be particularly sensitive to probe the modulation of an interfacial capacitor.[16] The schematic of Figure 2a also shows the ferroelectric-pattern-assisted XPS technique on the PZT (3.5 nm)/LAO (4 u.c.)/STO heterointerface. The binding energy of the Sr core level from the buried layer thus decreases ($E_B^{Sr} - eV_{up}$) or increases ($E_B^{Sr} + eV_{up}$), depending on the downward and upward polarization directions, respectively, in comparison to the binding energy of the Sr core level (E_B^{Sr}) from the LAO/STO heterointerface. Evidently, the concept of the interface capacitor is also confirmed by the lack of change of the core-level emissions from the top PZT (Pb 4f core level) and LAO (La 4d and Al 2s core levels) layers. Figure 2b shows the characteristic core-level photoelectron spectra in the ferroelectric PZT/LAO/STO and conducting LAO/STO heterointerface samples. The binding energy of Sr $3d_{5/2}$ core-level shifts associated with the potential drops of the PZT-modulated LAO/STO interface capacitors were obtained at values of +0.15 eV (P_{up} state) and –0.1 eV (P_{down} state), and the core-level differences between Sr $3d_{5/2}$ and La $4d_{5/2}$ (ΔE_{CL}) were determined to be 31.15 eV (P_{up} state) and 30.90 eV (P_{down} state).

The modulation of the electronic structure of the LAO/STO heterointerface by ferroelectric polarization was further developed by performing XSTM/S measurements on a sample with a thick PZT top layer (20 nm). The variations of the electronic structure across the heterointerface produce corresponding variations in the current–voltage behavior of scanning tunneling spectroscopy (STS) measurements. Therefore, a sample that was cleaved in situ in the STM chamber was kept under a background pressure of less than 1×10^{-10} Torr and cooled it down to ca. 100 K so that spatially resolved STS based on the XSTM image could reveal directly the electronic structure of the heterostructures. **Figure 3**a shows the XSTM image across the heterostructured interface, and the colored bars indicate the positions where STS measurements were performed. The different regions of Nb-STO, STO, LAO, and PZT layers were identified from the tunneling current image, which reveals specific electronic characteristics of each layer. Figures 3b and c show the evolution of the electronic structures of LAO from a position near the STO side (N), via the middle of LAO (M), to a position away from STO (A) in the naturally P_{up} and poled P_{down} samples, respectively. In the STS results, to exclude the effects

© 2013 WILEY-VCH Verlag GmbH & Co. KGaA, Weinheim

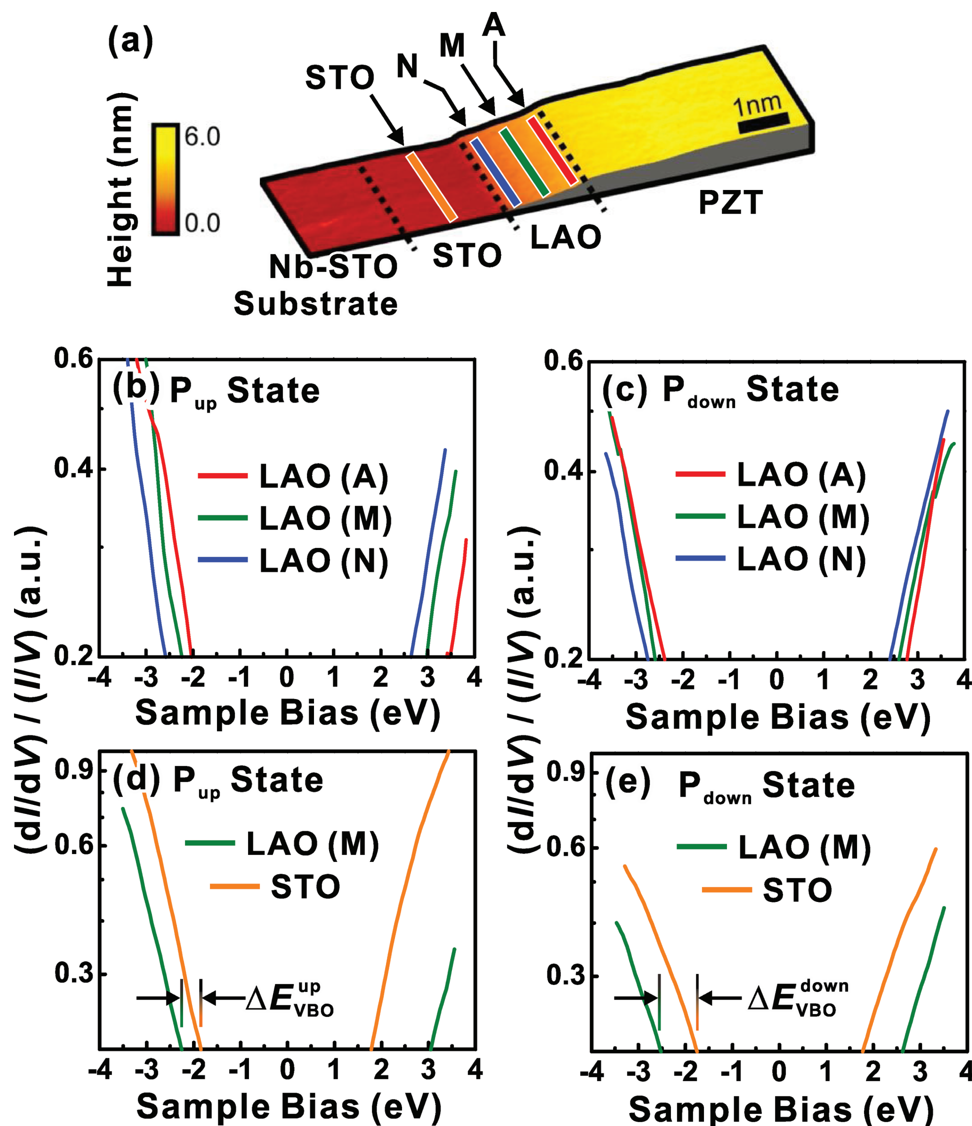

Figure 3. a) A typical cross-sectional constant-current STM image of the epitaxial PZT/LAO/STO heterostructure. b,c) The spatial spectroscopic measurements on LAO surfaces of PZT/LAO/STO systems for b) the downward-polarized (P_{up}) and c) the upward-polarized (P_{down}) situation in PZT films for a position in LAO near the STO side (N), the middle of LAO (M), and a position in LAO away from STO (A). d,e) The average spatial spectroscopic measurements on LAO (green curve) and STO (orange curve) surfaces for d) the downward-polarized (P_{up}) and e) the upward-polarized (P_{down}) situation in PZT films.

of surface and gap states in LAO and STO layers, which disturb band edge determination,[17] current offsets larger than 0.2 A at negative/positive sample biases are indicated as the energetic positions of the valence band maximum (VBM) and conduction band minimum (CBM). Therefore, the comparison of the energy shifts of the band edges can be referred to not only the value of the electric field in LAO but also the energetic shift across the interface from STO to LAO. As shown in Figures 3b and c, the energy shift of the band edges in LAO is smaller for the P_{down}-state sample than that for the P_{up}-state sample, indicating that the electric field in the LAO layer diminishes when the polarization of PZT is switched from the natural P_{up} state to the P_{down} state. Furthermore, according to the energy shifts between STO and LAO, as shown in Figures 3d and e, the suppressed electric field in LAO corresponds to the increase of valence band offset (VBO) value from ≈0.5 eV (P_{up}) to ≈1.0 eV (P_{down}) of the LAO/STO electronic structure. For comparison with the XPS measurements of the heterojunction as shown above, we measured the energy difference between the characteristic core level and the VBM of each layer, which is a material constant; the polarization-switching-induced Sr core-level shift is thus related directly to the VBO change of the LAO/STO heterostructure. Therefore, the VBO variation of the LAO/STO sample modulated by a thin PZT layer (3.5 nm) is about 0.25 eV, as obtained by XPS, which is smaller than that of LAO/STO capped with a thick PZT layer (20 nm), which is ≈0.5 eV, obtained by STS. In both ferroelectric-pattern-assisted spectral results, we find that the presence of up- and down-polarized

© 2013 WILEY-VCH Verlag GmbH & Co. KGaA, Weinheim

PZT layers would induce additional interface electrostatics and eventually lead to a change of the VBO of the LAO/STO heterostructure. The change of VBO depends on the thickness of the top PZT layer, which ranges from 3.5 nm to 20 nm (with a wide polarization range from 11 μC cm^{-2} to above 100 μC cm^{-2} reported in defect-free films),[18–21] leading to an increase from 0.25 eV to 0.5 eV, and the response of VBO change on ferroelectric polarization switching is consistent (P_{up} PZT increases the VBO value of LAO/STO, in contrast to P_{down} PZT).

To explore the phenomenon of the ferroelectricity of PZT at the LAO/STO interface associated with its band structure, we studied the E_c band bending (invert electronic potential bending), bound and free charge concentration, and the electronic conductivity inside the effective length of the STO layer under P_{up} and P_{down} states of PZT using a phase-field approach. First, the static profiles of the potential and electrons within the STO layer in the absence of PZT polarization were obtained by solving the following coupled equations in the steady state:

$$\nabla^2\psi = -\frac{\rho}{\varepsilon_0\varepsilon_r} = \frac{e_0 n}{\varepsilon_0\varepsilon_r} \tag{1}$$

$$\frac{\partial n}{\partial t} = -\nabla J = D\nabla^2 n - \mu\nabla(n\nabla\psi) \tag{2}$$

where ψ is the electric potential, ρ the charge density, e_0 the unit charge, n the electron concentration, ε_0 the vacuum permittivity, and ε_r the dielectric constant of STO. D and μ stand for the diffusivity and mobility, respectively, of electrons in STO. It is seen that the band bending at the STO/LAO interface (without a PZT layer on top) is about 0.3 eV, which causes electron accumulation at the interface (shown in **Figure 4**a).

In the presence of PZT polarization, the bound charge induced by the polarization and electric potential drop at the PZT/LAO interface is estimated by introducing $\rho = -\nabla P$. At the PZT/LAO interface, where the polarization reduces to 0, a negative bound charge sheet is formed in the case of P_{up} polarization in the PZT layer. Based on the Poisson equation, we have

$$\nabla^2\psi = \frac{\nabla P_i}{\varepsilon_0\varepsilon_r} \tag{3}$$

The electric potential drop at the PZT/LAO interface due to the PZT P_{down} bound charge is calculated to be about –0.5 V. Since electric potential should be continuous throughout the heterostructure, the potential decrease through the STO and LAO layers should be equal to the potential drop at the PZT/LAO interface. In addition, the effective length within STO is about 0.8 nm while the thickness of the LAO layer is about 1.1 nm. The potential drop at the LAO/STO interface can be estimated using

$$\begin{aligned}\Delta V_{total} &= \Delta V_{LAO/STO} + \Delta V_{LAO} \\ &= \left(\frac{a_{STO}^{eff}}{a_{STO}^{eff} + a_{LAO}}\right)\Delta V_{total} + \left(\frac{a_{LAO}}{a_{STO}^{eff} + a_{LAO}}\right)\Delta V_{total}\end{aligned} \tag{4}$$

where $\Delta V_{LAO/STO}$ and ΔV_{LAO} stand for potential drop at the LAO/STO interface and inside LAO, respectively. a_{STO}^{eff} and a_{LAO} are the effective length within STO and thickness of LAO, respectively. Therefore, in the case of P_{up} polarization in the PZT layer, the potential decreases by 0.2 V at the LAO/STO interface, and thus interface E_C band bending decreases from –0.3 eV to –0.1 eV. On the other hand, when the PZT polarization is P_{down}, a positive sheet of bound charges is formed at the PZT/LAO interface, which increases the local potential at the PZT/LAO interface and leads to the increase of the E_C band bending at the LAO/STO interface from –0.3 eV to –0.5 eV (shown in Figure 4a).

Furthermore, the electron concentration and the electronic conductivity inside the effective length of the STO layer have been calculated and summarized in Figure 4b. Clearly, the polarization in the PZT layer has a significant effect on the electron concentration and conductivity σ on the STO side of the LAO/STO interface, where the electronic conductivity is calculated by $\sigma = ne_0\mu$. The electron concentration away from the LAO/STO interface region is ca. 10^9 cm^{-3}. When the ferroelectric polarization inside the PZT layer is down (P_{down}), the electron accumulation is significant, reaching up to 10^{18} cm^{-3}, with band bending of about 0.5 eV in the vicinity of the LAO/STO interface. Furthermore, the local conductivity is calculated to be ca. 10^0 Ω^{-1} cm^{-1}, indicating that the interface becomes more conducting (Figure 4b). The electron accumulation is strongly inhibited (ca. 10^{11} cm^{-3}) when the polarization in the PZT layer is P_{up}, with interface band bending of 0.1 eV. In this case the interface becomes less conducting, with local conductivity of ca. 10^{-7} Ω^{-1} cm^{-1}.

Based on the phase-field modeling results, which agree well with the experimental observations of ferroelectric-pattern-assisted transport measurements and XPS and XSTS spectra, we display the mechanism of ferroelectric modulation of LAO/STO conductivity in Figure 4c. In the case of the natural P_{up} state of capped PZT, because the bottom of the PZT layer has a negative polarization charge sheet, the potential buildup in the polar LAO layer increases and the free electrons are repelled from the LAO/STO interface (electron depletion), where the interface band bending of the STO side decreases with smaller VBO value and makes ΔE_{CL} larger. When the polarization is switched to the P_{down} state, the positive polarization charge sheet at the bottom of the PZT layer makes the LAO potential buildup decrease and attracts more free electrons to the LAO/STO interface (electron accumulation), where the interface band bending of the LAO side increases with larger VBO value and smaller ΔE_{CL}. In addition, for the LAO/STO heterostructure with a thin LAO layer (3 u.c.), the variation of electric potential induced by E_{PZT} can be estimated to be about 1.0 eV, in that the thickness of the LAO layer is about 1.1 nm (3 u.c.) and the stray electric field in the LAO layer is estimated to be about 10^9 V m^{-1}, as shown in the Supporting Information (Figure B1b). This 1.0 eV potential variation is three times larger than the built-in potential variation (about 0.3 eV) from the metal–insulator transition proposed in previous results.[7,21,22] Therefore, thanks to the reversible polarization of the top ferroelectric layer, the PZT/LAO/STO system is expected to be the one closest to having non-volatile switching on/off characteristics at the LAO/STO interface.

Moreover, in the calculation results, the change of band bending at the LAO/STO interface caused by the PZT layer changing from the P_{up} state to the P_{down} state is around 0.4 eV (Figure 4a), which results in higher conductivity at the interface with a conductivity ratio of about 10^7 (Figure 4b). In the

© 2013 WILEY-VCH Verlag GmbH & Co. KGaA, Weinheim

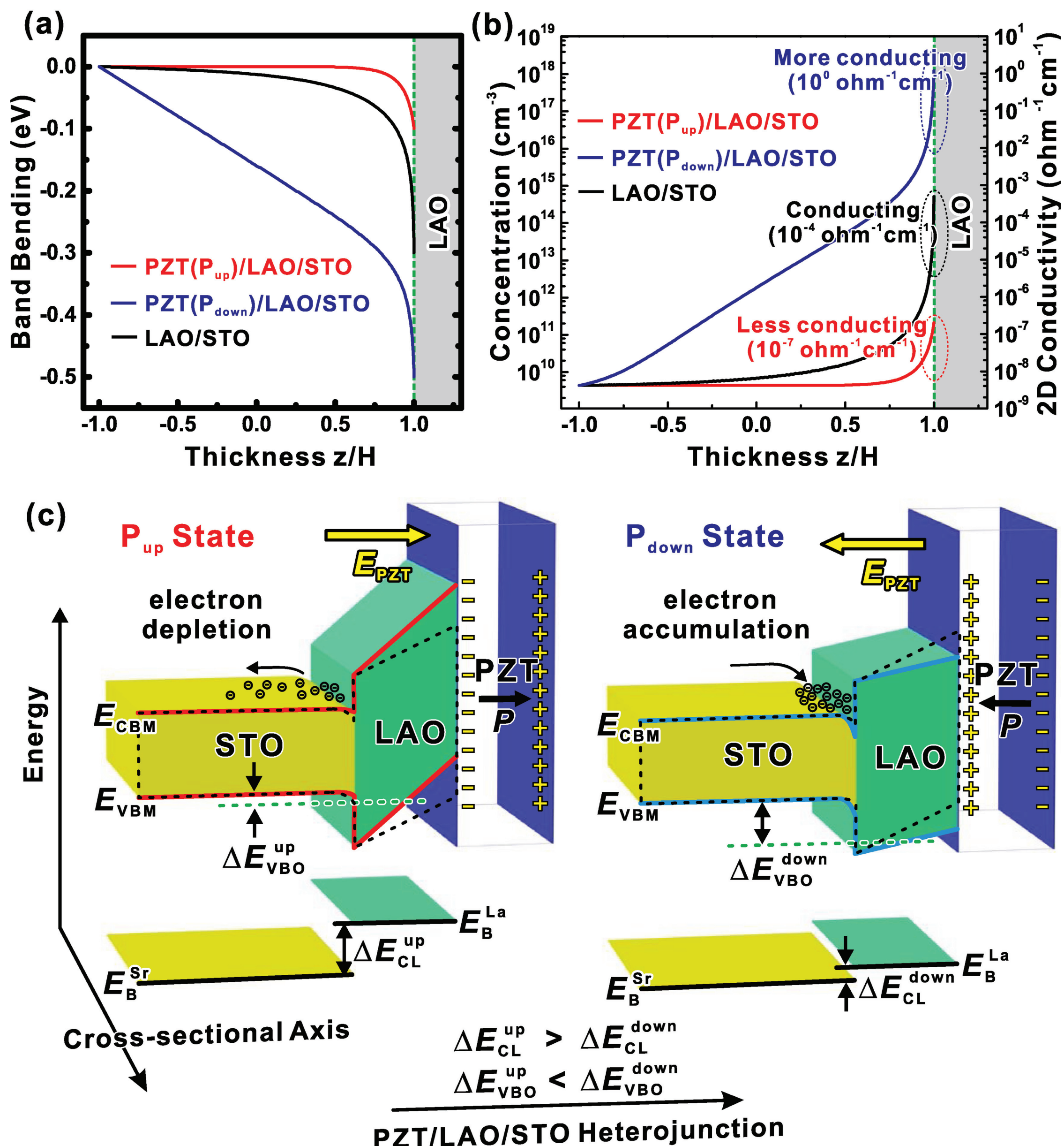

Figure 4. E_c band bending (a) and electron concentration and local electronic conductivity (b) in the STO layer in the presence of upward polarization, no polarization, and downward polarization in the PZT layer (z denotes the position in the STO layer and H is half of the layer thickness, so that z/H from −1 to +1 represents the entire layer). c) Schematic band diagrams of a PZT/LAO/STO heterointerface derived from ferroelectric-pattern-assisted XPS and XSTM/S measurements. The sheet of negative/positive bound charges at the bottom of the PZT layer and its induced E-field (E_{PZT}) across the LAO layer would directly affect the depletion/accumulation of the mobile charges at the LAO/STO heterointerface, which are shown for both polarization states (P_{up} and P_{down}) of the PZT layer. Decreased and increased buildup of potential across the LAO layer corresponding to the different polarization states is indicated. Combining both XPS and STS spectroscopic results, the changes in valence band offset (ΔE_{VBO}) and core-level energetic separation (ΔE_{CL}) between the LAO and STO layers are revealed, and allow a ferroelectricity-modulated LAO/STO band structure model to be constructed.

transport results shown in Figure 1, on going from the PZT P_{up} state to P_{down} state an experimentally measured conductivity ratio of about 10^3 was obtained in the PZT (20 nm)/LAO (3 u.c.)/STO sample (Figure 1d), which reveals PZT-induced switching on/off capability at the LAO/STO interface. However, based on the numerical calculation, a local conductivity ratio of 10^3 corresponds to a band bending change of 0.2 eV. This change value is smaller than the band offset shifts obtained from STM of about 0.5 eV, which is shown in Figure 3, with the same PZT thickness of 20 nm. The differences in band edge shifts and conductivity ratio (from P_{up} to P_{down}) between experimental and theoretical results can be attributed to the spatial resolution limit in XPS and XSTM measurements and the simplified bound/free charge modeling at PZT/LAO and LAO/STO interfaces. Here, the changes in band bending profile at the interface were evaluated by monitoring the changes

© 2013 WILEY-VCH Verlag GmbH & Co. KGaA, Weinheim

in VBO. The variation of band bending value at the interface was assumed to be smaller than the VBO shift, owing to the free carriers at the LAO/STO interface that would compensate polarization field effects. Additionally, in the theoretical calculation, the partial compensations at the PZT/LAO and LAO/STO interfaces were set to zero to simplify the modeling. This makes the theoretical predictions of the electric potential, band bending, and resistivity ratio larger than the experimental results.

In conclusion, we have demonstrated that ferroelectric polarization can tune and modulate the conduction at the LAO/STO heterointerface. The XPS and XSTM/S results reveal the electrostatic predictions of the conducting state modulation, demonstrate the possibility of non-volatile control, and provide compelling evidence in favor of ferroelectric doping at the conducting polar/nonpolar oxide heterointerface.

Experimental Section

Sample Preparation: To realize the LAO/STO interface, a TiO_2-terminated STO(100) substrate was used for this study. An atomically smooth surface with clear u.c. height steps was observed with atomic force microscopy (AFM). On top of that, LAO and PZT were grown by pulsed laser deposition assisted by high pressure reflection high-energy electron diffraction (RHEED). The substrate was heated to 850 °C and maintained at this temperature during the LAO growth at 2×10^{-5} Torr oxygen pressure. LAO thin films were grown successfully with the layer-by-layer growth mode. After that, the samples were cooled down to 620 °C and oxygen pressure was tuned to 120 mTorr to start the growth of the PZT layer. After growth, the samples were annealed for 30 min and cooled to room temperature in O_2 at a pressure of 600 Torr.

Structural and Electrical Transport Characterization: X-ray diffraction techniques were employed to investigate the thin film structure. The θ–2θ scan and the asymmetric reciprocal space maps (RSMs) were performed using the synchrotron radiation source beamline BL-17A at the National Synchrotron Radiation Research Center (NSRRC) in Hsinchu, Taiwan. The incident beam was monochromated at 9.3 keV (ca. 1.333 Å) with a Si(111) double crystal mirror and then focused by a toroidal focusing mirror to obtain a higher intensity beam. Four sets of slits were used to gain the detection resolution, where two sets of slits were placed in front of the samples to set beam size about 0.5 mm × 1 mm and the other two were placed after the sample (or before the scintillation counter) to decrease background noise. These diffraction measurements were then plotted in reciprocal lattice units normalized to the STO substrate (1 r.l.u. = $2\pi/a_{STO}$).

In order to conduct the transport measurements, four square metallic (Au/Ti) electrodes (0.3 mm^2 size) connected to the LAO/STO interface were thermally evaporated on each of the PZT/LAO films using e-beam lithography. Then gold wires were manually bonded to the electrodes using silver paste. The samples were cooled by closed cycle refrigeration and the transport measurements were carried out in a physical property measurement system (PPMS) (Quantum Design) from room temperature to 20 K.

XSTM and XPS: For STM studies, the sample was cleaved in situ and measurements were performed in the cross-sectional geometry in an ultrahigh vacuum (UHV) chamber with a base pressure of ca. 5×10^{-11} Torr. In addition, STS images were simultaneously acquired at ca. 100 K temperature. XPS spectra were collected at room temperature on a Thermo Scientific K-Alpha system, equipped with a monochromatized Al Kα X-ray source of 1486.6 eV. The C 1s signal at 284.6 eV was used as the energy reference to correct for charging. The standard deviation of the XPS peak position errors is about 16 meV, which is smaller than the step size of 50 meV used for the acquisition.

Supporting Information

Supporting Information is available from the Wiley Online Library or from the author.

Acknowledgements

This work was supported by the National Science Council of the Republic of China (under contract no. NSC-101-2119-M-009-003-MY2 and NSC 100-2112-M-006-010-MY3), the Ministry of Education (grant no. MOE-ATU 101W961), the Center for Interdisciplinary Science at National Chiao Tung University, and the Headquarters of University Advancement at National Cheng Kung University. The work at Penn State University was supported by the Department of Energy, Basic Sciences, under DE-FG02-07ER46417. L.Q.C., A.N.M., and E.A.E. acknowledge the financial support via the bilateral SFFR-NSF project (US National Science Foundation under NSF-DMR-1210588 and the State Fund of Fundamental State Funds of Fundamental Research of Ukraine, grant UU48/002).

Received: February 16, 2013
Published online: May 13, 2013

[1] H. Y. Hwang, Y. Iwasa, M. Kawasaki, B. Keimer, N. Nagaosa, Y. Tokura, *Nat. Mater.* **2012**, *11*, 103–113.
[2] P. Zubko, S. Gariglio, M. Gabay, P. Ghosez, J.-M. Triscone, *Annu. Rev. Condens. Matter Phys.* **2011**, *2*, 141–165.
[3] A. Ohtomo, H. Y. Hwang, *Nature* **2004**, *427*, 423–426.
[4] N. Nakagawa, H. Y. Hwang, D. A. Muller, *Nat. Mater.* **2006**, *5*, 204–209.
[5] N. Reyren, S. Thiel, A. D. Caviglia, L. F. Kourkoutis, G. Hammerl, C. Richter, C. W. Schneider, T. Koop, A.-S. Rüetschi, D. Jaccard, M. Gabay, D.A. Muller, J.-M. Triscone, J. Mannhart, *Science* **2007**, *317*, 1196–1199.
[6] A. Brinkman, M. Huijben, M. van Zalk, J. Huijben, U. Zeitler, J. C. Maan, W. G. van der Wiel, G. Rijnders, D. H. A. Blank, H. Hilgenkamp, *Nat. Mater.* **2007**, *6*, 493–496.
[7] S. Thiel, G. Hammerl, A. Schmehl, C. W. Schneider, J. Mannhart, *Science* **2006**, *313*, 1942–1945.
[8] A. D. Caviglia, S. Gariglio, N. Reyren, N. Jaccard, T. Schneider, M. Gabay, S. Thiel, G. Hammerl, J. Mannhart, J.-M. Triscone, *Nature* **2008**, *456*, 624–627.
[9] G. Singh–Bhalla, C. Bell, J. Ravichandran, W. Siemons, Y. Hikita, S. Salahuddin, A. F. Hebard, H. Y. Hwang, R. Ramesh, *Nat. Phys.* **2011**, *7*, 80–86.
[10] G. Cheng, P. F. Siles, F. Bi, C. Cen, D. F. Bogorin, C. W. Bark, C. M. Folkman, J.-W. Park, C.-B. Eom, G. Medeiros-Ribeiro, J. Levy, *Nat. Nanotechnol.* **2011**, *6*, 343–347.
[11] Y. Xie, C. Bell, T. Yajima, Y. Hikita, H. Y. Hwang, *Nano Lett.* **2010**, *10*, 2588–2591.
[12] C. Cen, S. Thiel, G. Hammerl, C. W. Schneider, K. E. Andersen, C. S. Hellberg, J. Mannhart, J. Levy, *Nat. Mater.* **2007**, *7*, 298–302.
[13] C. W. Bark, P. Sharma, Y. Wang, S. H. Baek, S. Lee, S. Ryu, C. M. Folkman, T. R. Paudel, A. Kumar, S. V. Kalinin, A. Sokolov, E. Y. Tsymbal, M. S. Rzchowski, A. Gruverman, C. B. Eom, *Nano Lett.* **2012**, *12*, 1765–1771.
[14] F. Bi, D. F. Bogorin, C. Cen, C. W. Bark, J.-W. Park, C.-B. Eom, J. Levy, *Appl. Phys. Lett.* **2010**, *97*, 173110.
[15] P. Yu, W. Luo, D. Yi, J. X. Zhang, M. D. Rossell, C.-H. Yang, L. You, G. Singh–Bhalla, S. Y. Yang, Q. He, Q. M. Ramasse, R. Erni, L. W. Martin, Y. H. Chu, S. T. Pantelides, S. J. Pennycook, R. Ramesh, *Proc. Natl. Acad. Sci. USA* **2012**, *109*, 9710–9715.
[16] C. L. Wu, P. W. Lee, Y. C. Chen, L. Y. Chang, C. H. Chen, C. W. Liang, P. Yu, Q. He, R. Ramesh, Y. H. Chu, *Phys. Rev. B* **2011**, *83*, 020103(R).

© 2013 WILEY-VCH Verlag GmbH & Co. KGaA, Weinheim

[17] B. C. Huang, Y. P. Chiu, P. C. Huang, W. C. Wang, V. T. Tra, J. C. Yang, Q. He, J. Y. Lin, C. S. Chang, Y. H. Chu, *Phys. Rev. Lett.* **2012**, *109*, 246807.

[18] V. Nagarajan, J. Junquera, J. Q. He, C. L. Jia, R. Waser, K. Lee, Y. K. Kim, S. Baik, T. Zhao, R. Ramesh, P. Ghosez, K. M. Rabe, *J. Appl. Phys.* **2006**, *100*, 051609.

[19] I. Vrejoiu, G. Le Rhun, L. Pintilie, D. Hesse, M. Alexe, U. Gösele, *Adv. Mater.* **2006**, *18*, 1657–1661.

[20] C.-L. Jia, V. Nagarajan, J.-Q. He, L. Houben, T. Zhao, R. Ramesh, K. Urban, R. Waser, *Nat. Mater.* **2007**, *6*, 64–69.

[21] Y. Segal, J. H. Ngai, J. W. Reiner, F. J. Walker, C. H. Ahn, *Phys. Rev. B* **2009**, *80*, 241107.

[22] J. W. Park, D. F. Bogorin, C. Cen, D. A. Felker, Y. Zhang, C. T. Nelson, C. W. Bark, C. M. Folkman, X. Q. Pan, M. S. Rzchowski, J. Levy, C. B. Eom, *Nat. Commun.* **2010**, *1*, 94.

© 2013 WILEY-VCH Verlag GmbH & Co. KGaA, Weinheim